PIER

Lymph Node Diagnosis for Colorectal Cancer by Utilizing a Hyperspectral Laparoscope and Machine Learning

Changwei Jiao[1, 2], Miaoliang Chen[2], Zehai Li[4], Jinbo Chen[2],
Jiaqi Liao[1, 2], Ruili Zhang[2, *], and Sailing He[2, 3, *]

[1] *Centre for Optical and Electromagnetic Research, College of Optical Science and Engineering*
Zhejiang University, Hangzhou 310058, China
[2] *Zhejiang Engineering Research Center for Intelligent Medical Imaging, Sensing and Non-invasive Rapid Testing, Taizhou Hospital*
Zhejiang University, Taizhou, China
[3] *National Engineering Research Center for Optical Instruments, Zhejiang University, Hangzhou 310058, China*
[4] *School of Computer Science and Technology, Zhejiang Normal University, Jinhua 321004, China*

ABSTRACT: We have developed a hyperspectral laparoscope capable of hyperspectral imaging during surgery. Using this hyperspectral laparoscope, we acquired hyperspectral images of fresh lymph nodes during colorectal cancer surgery. By integrating an improved U-Net algorithm specifically tailored for hyperspectral imaging, we achieved a recognition accuracy of 94%. Our results demonstrate that the multimodal hyperspectral imaging system has a great advantage and potential in label-free intraoperative diagnosis of lymph node metastasis in colorectal cancer.

1. INTRODUCTION

Colorectal cancer (CRC) ranks as the third most common malignant tumor globally [1]. Significant disparities in incidence and mortality rates exist between developed nations and those undergoing economic transition. For the foreseeable future, the number of patients with CRC will constitute a substantial proportion of the malignant tumor patient population. While personalized treatment can improve the survival of CRC patients, the timing of optimal diagnosis and treatment for patients with advanced and recurrent CRC is often delayed due to technological limitations and insufficient patient health awareness [2]. These delays lead to poor prognoses and restricts the overall improvement in the diagnosis and treatment of CRC.

Common diagnostic methods for CRC include physical examination, laboratory tests, colonoscopy, imaging, and pathological examination [3]. The poor prognosis of patients is partly due to concealed early symptoms, which often go unnoticed until the disease has progressed, and partly because the surgical treatment for advanced CRC is limited in effectiveness, with postoperative recurrence and metastasis being major challenges. Accurate identification of metastatic lymph nodes; number and location is crucial for guiding precise lymph node dissection during surgery, which is vital for treatment and improving postoperative outcomes related to recurrence and metastasis. Metastatic lymph node-directed personalized and precise surgery holds promise for advancing CRC treatment.

Thorough dissection of metastatic lymph nodes is essential to ensure the effectiveness of CRC surgery, but identifying the nature of lymph nodes intraoperatively is extremely challeng-

ing. Extensive research has been conducted in preoperative and intraoperative lymph node localization and prediction [4]. The current focus is on lymph node tracing techniques, which involve using various tracers to identify lymph nodes in the tumor drainage area. The main methods are nuclear tracing, dye tracing, and fluorescence tracing. The use of radioactive colloids and dyes for sentinel lymph node (SLN) tracing in clinical settings has limitations. The drawbacks of using radioactive colloids for lymph node localization include radiation exposure to medical staff, issues with radioactive material disposal, high medical costs, and restricted access to radioactive isotopes [5]. Dye tracing methods, such as methylene blue, nano carbon, isosulfan blue, and patent blue, also have limitations, including potential allergic reactions, high false-negative rates, poor visibility in dense adipose tissue, and inadequate accumulation and retention in lymph nodes [6, 7]. Fluorescence tracing holds significant promise for improving the detection sensitivity of metastatic lymph nodes. Traditional fluorescence tracers, such as indocyanine green (ICG) and methylene blue, can sensitively display lymph nodes but still face issues like dye color interference in the surgical field, low accumulation, and short retention times, which affect tracing effectiveness. Therefore, multifunctional fluorescent nanoprobes have been developed to overcome these limitations. With the advent of the AI era and the advancements in healthcare information technology, deep neural network methods have been applied to predict lymph node metastasis throughout the CRC treatment cycle [8]. However, each lymph node tracing technique has its drawbacks, and there is an urgent need to develop more ideal methods for predicting and locating metastatic lymph nodes.

---

* Corresponding authors: Sailing He (sailing@zju.edu.cn); Ruili Zhang (zhangrl@enzemed.com).

Hyperspectral imaging is a rapid, noninvasive technique that can simultaneously acquire spatial and spectral information of tissue structures, providing multidimensional information about cells, including morphology, structure, chemical composition, and function, thereby enhancing the accuracy and sensitivity of cancer cell identification. Waterhouse et al. [9] combined spectral endoscopy with AI algorithms to achieve 84.8% accuracy, 83.7% sensitivity, 85.5% specificity, 78.3% positive predictive value, and 89.4% negative predictive value in the detection of neoplasia in Barrett's esophagus. Our research group has developed hyperspectral imaging by tunable liquid crystal filters [10], and utilized hyperspectral imaging for detecting the freshness of meat [11]. Yoon et al. [12] developed a hyperspectral endoscopy system that can simultaneously record *in vivo* hyperspectral and standard white-light images, compensating for image distortions and reconstructing accurate hyperspectral data cubes during endoscopic movement, showing significant potential in the diagnosis of colorectal diseases. Kumashiro et al. [13] developed an integrated endoscopic system based on optical imaging and hyperspectral data analysis, achieving a differentiation rate of 72.5% between tumor and non-tumor tissues with a sensitivity of 82.1% and a specificity of 82.1%.

In this study, we developed a multimodal hyperspectral imaging system, along with control software to facilitate clinical use. We also introduced an optimized version of the U-Net algorithm for hyperspectral data. The system was used to image 80 fresh lymph node samples obtained during CRC surgery, achieving a recognition accuracy of 97.68%. When we integrated our hyperspectral imaging system with a commercial laparoscopy and applied it to fresh surgical specimens, we achieved a testing accuracy of 94%. These results demonstrate that our system outperforms conventional laparoscopic examinations and has significant potential for *in vivo*, label-free diagnosis of lymph node metastasis in CRC.

2. MATERIALS AND METHODS

2.1. Sample Preparation

The samples were collected from patients who underwent surgery at Taizhou Hospital, Zhejiang Province, in 2024. All patients included in the study had complete medical records and met the inclusion and exclusion criteria. This study adhered to ethical standards for human trials and was approved by the hospital's ethics committee [Ethics Approval Number: K20241055]. The inclusion criteria were: patients who visited Taizhou Hospital, postoperative tissue samples confirmed by histopathological examination, and tissue samples preserved in good condition before spectral detection.

For the obtained tissue samples, they were first rinsed thoroughly with physiological saline to remove blood and other contaminants, then dried with gauze and placed on the testing platform for hyperspectral imaging acquisition. After spectral detection, the samples were immediately fixed in 10% formalin solution, embedded in paraffin, and sectioned for subsequent hematoxylin and eosin (H&E) staining and pathological analysis.

In total, this experiment involved the examination of 80 lymph nodes from 15 patients in the colorectal cancer region, including 23 lymph nodes with tumor metastasis and 57 normal lymph nodes.

2.2. System Setup and Data Acquisition

The system includes a Fiberoptic Imaging Connector that can directly connect to the hospital's laparoscope. In this work, we integrated our system with both our custom imaging lens and a commercially available high-definition laparoscope (M01030A, Mindray, China) to set up the equipment. The specific optical path diagram is shown in Figure 1(a), which allows simultaneous RGB and hyperspectral imaging.

To facilitate data acquisition by clinical personnel, we developed a control software program (based on LabVIEW, National Instruments, USA). The software interface is shown in Figure 1(b) and includes features such as controlling camera acquisition parameters, controlling the LCTF (Liquid Crystal Tunable Filter) parameters, saving the acquired multimodal data, and displaying the acquired data.

After setting up the hardware and software of the equipment, we began data collection. We wheeled the equipment into the operating room and waited for the lymph node samples that had just been removed. We cleaned the surface of the lymph nodes with deionized water to remove any blood and other contaminants, and then used gauze to absorb excess water from the samples. The samples were placed on a sample stage with a light-shielding cover, and the light source was turned on. We collected data with the following settings: Camera 1 had an integration time of 100 ms to capture the RGB images of the samples, while Camera 2 had an integration time of 150 ms to acquire the hyperspectral information of the same regions.

As shown in Figure 2, the average spectra of metastatic lymph nodes differ from those of healthy lymph nodes. However, the spectra of individual regions exhibit some overlap. Therefore, we need to combine the hyperspectral data with artificial intelligence algorithms to utilize both the spectral and spatial information, enabling more accurate and stable identification.

2.3. Data Processing

For the obtained multimodal hyperspectral data, we need to perform identification using artificial intelligence algorithms. We have adopted an improved U-Net algorithm specifically designed for hyperspectral imaging data. The original U-Net architecture consists of an encoder, a decoder, and skip connections. The encoder performs downsampling feature extraction using convolutional layers and pooling layers. Each downsampling module first undergoes a max pooling operation (size 2×2), followed by two convolutions (size 3×3), doubling the number of channels during the downsampling process. The structure includes four layers of downsampling modules. The decoder performs upsampling to restore the feature map size. Each upsampling module first enlarges the size through interpolation, followed by two convolutions (size 3×3) to complete the upsampling process, halving the number of channels during
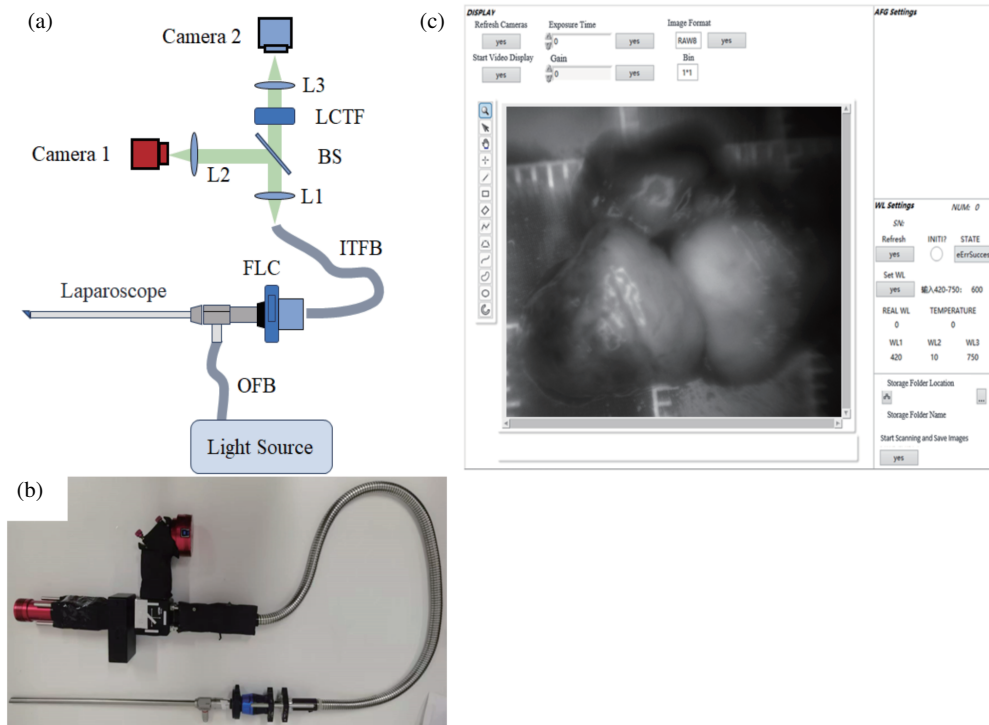
FIGURE 1. (a) Optical path diagram of the multimodal hyperspectral laparoscope, where: ITFB: Image-Transmitting Fiber Bundle; L: Lens; BS: Beam Splitter; LCTF: Liquid Crystal Tunable Filter; FLC: Fiberoptic Laparoscope Connector. (b) We developed a user-friendly acquisition software using LabVIEW (National Instruments, USA) to enable one-button data collection for clinical personnel; (c) An image of a multimodal hyperspectral laparoscope.
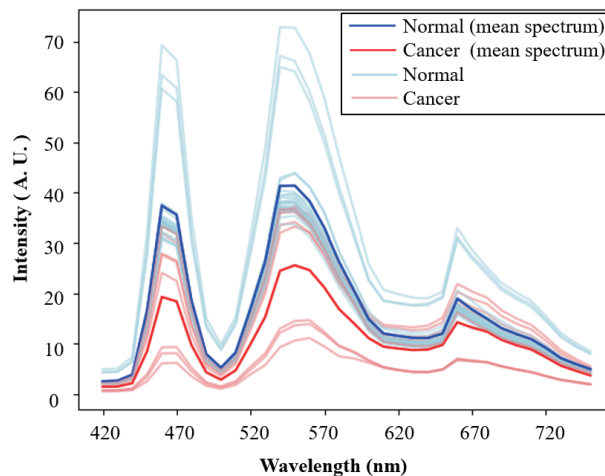

FIGURE 2. The reflectance hyperspectral test results of the lymph nodes include the spectra and their average spectra for both healthy and metastatic lymph nodes.

upsampling. Skip connections are used to integrate corresponding features from the encoder and decoder.

Compared to pooling operations that directly take the maximum or average values, convolution operations during downsampling use convolutional kernels to weight and sum surrounding information, better preserving local details and avoiding information loss. Therefore, we have replaced the pooling operations in the downsampling process with convolutions.

Additionally, the original model lacks an attention mechanism. To enhance the segmentation performance, we have introduced the CBAM (Convolutional Block Attention Module) in the upsampling modules. The improved model structure is shown in Figure 3.

Attention is a method in machine learning used to process data, enabling neural networks to focus more on specific features and local information. It primarily consists of channel
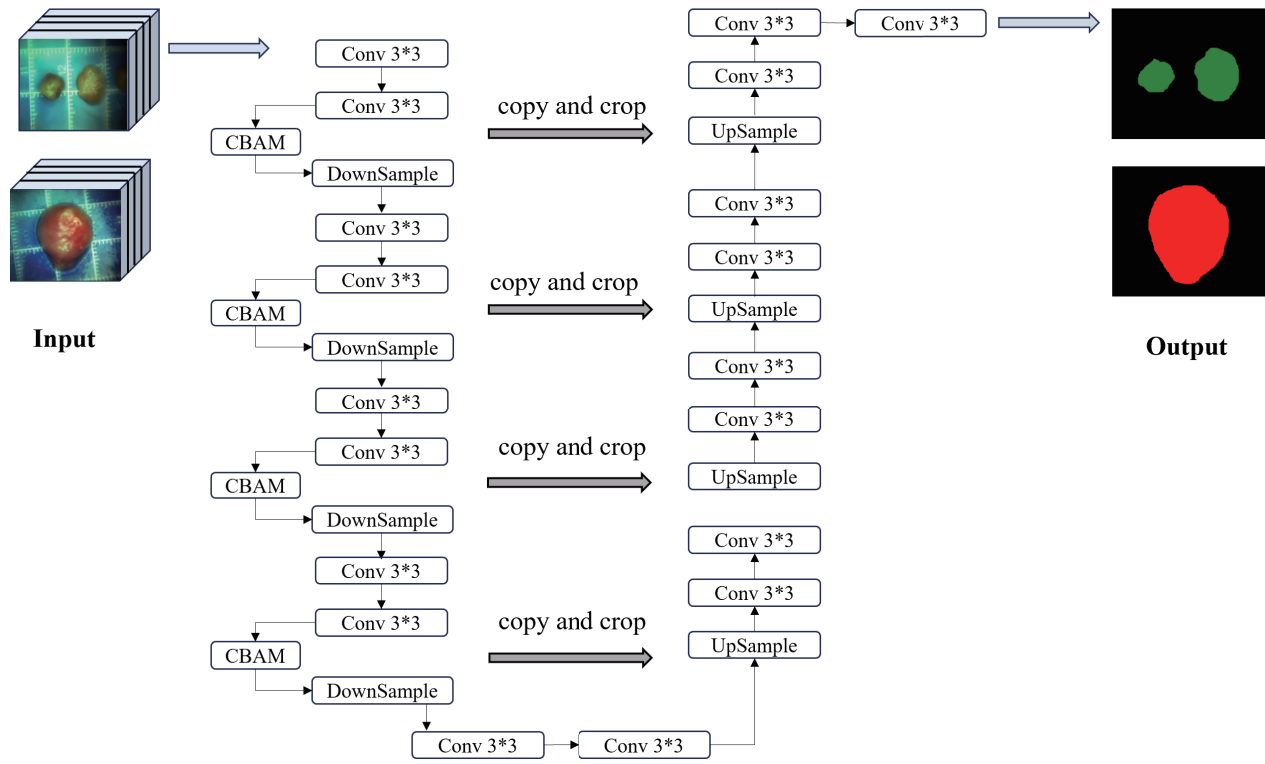
FIGURE 3. This paper adopts an improved version of the U-Net algorithm structure. Under the U-Net framework, the downsampling process uses convolutions instead of the original pooling operations, and an attention module is applied before each downsampling step.

attention and spatial attention. The Convolutional Attention Module (CBAM) integrates both the Channel Attention Module and the Spatial Attention Module. The structure of this model is shown in Figure 4.

Figure 4(a) shows the Convolutional Block Attention Module (CBAM), which integrates both the Channel Attention Module and the Spatial Attention Module. Figure 4(b) illustrates the Channel Attention Module. The intermediate feature map $M \in C \times H \times W$ serves as the input to this module. Two different spatial context descriptors are obtained through AvgPool and MaxPool operations. These two descriptors are then processed by a Multilayer Perceptron (MLP) to generate channel attention maps. The channel attention maps are summed element-wise to produce a feature vector. Finally, the feature vector is passed through a sigmoid activation function to generate the output. This process can be represented as:

$$O_c(M) = \sigma(\text{MLP}(\text{AvgPool}(M) + \text{MLP}(\text{MaxPool}(M)))$$

Here, σ denotes the sigmoid function, M the input to the channel attention module, and $O_c(M)$ the output of the channel attention module. Figure 4(c) illustrates the structure of the channel attention module. The output of this module is element-wise multiplied with the original input feature map, and the resulting feature map is fed into the spatial attention module. Then, the average and maximum values are computed along the channel dimension, like AvgPool and MaxPool operations. These two results are concatenated and passed through a standard convolution layer, followed by activation with the sigmoid function to generate the spatial attention map. This

process can be represented as:

$$O_s(M) = \sigma(f^{7\times 7}(\text{concat}(\text{AvgPool}(M), \text{MaxPool}(M))))$$

Here, σ denotes the sigmoid function; $f^{7\times 7}$ is a convolution operation with a 7×7 kernel; M is the input to the spatial attention module; and $O_s(M)$ is the output of the spatial attention module.

The above describes the structure of our algorithm used for processing multi-modal data. We input the obtained hyperspectral cube data into an improved U-Net algorithm for training and prediction. The training data consists of 7 groups of lymph nodes with metastatic tumors and 20 groups of normal lymph nodes. The testing data includes 8 groups of lymph nodes with metastatic tumors and 11 groups of normal lymph nodes. Note that all the test data were from some patients whose lymph nodes were never used in the training data.
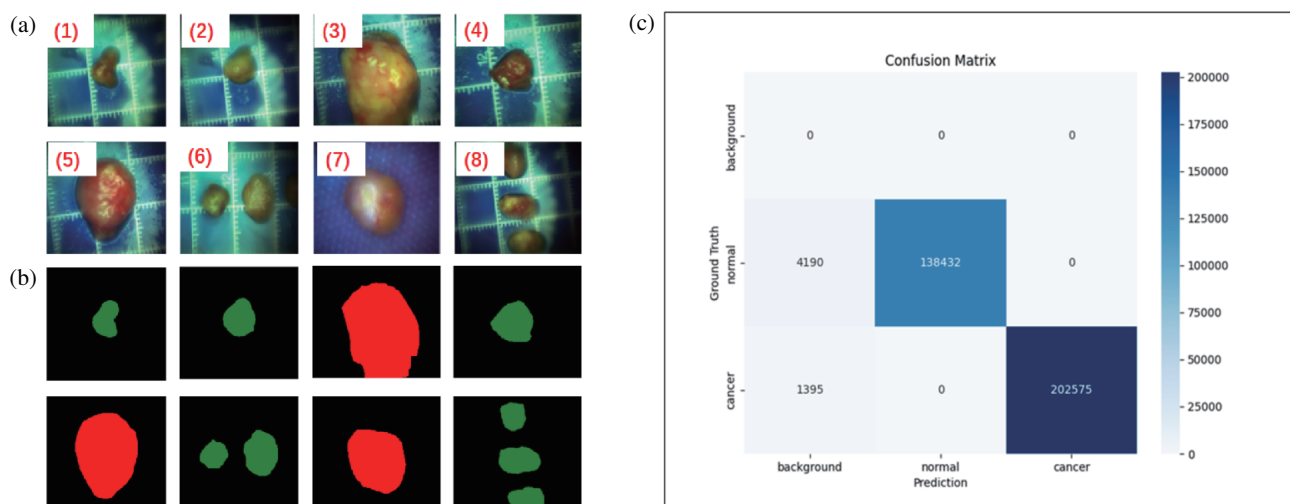
3. RESULTS AND DISCUSSION

In Figure 5(a), the RGB images of the testing lymph nodes are displayed, where (1), (2), (4), (6), and (8) are normal lymph nodes, and the others are lymph nodes with metastatic tumors. Figure 5(b) shows the recognition results when the hyperspectral cube is used as input. Figure 5(c) displays the confusion matrix of the recognition results using the hyperspectral cube as input, with an accuracy of 97.68%.

To further validate the potential of our system in clinical applications, we integrated our hyperspectral imaging system with a commercial laparoscopy and applied it to fresh surgical
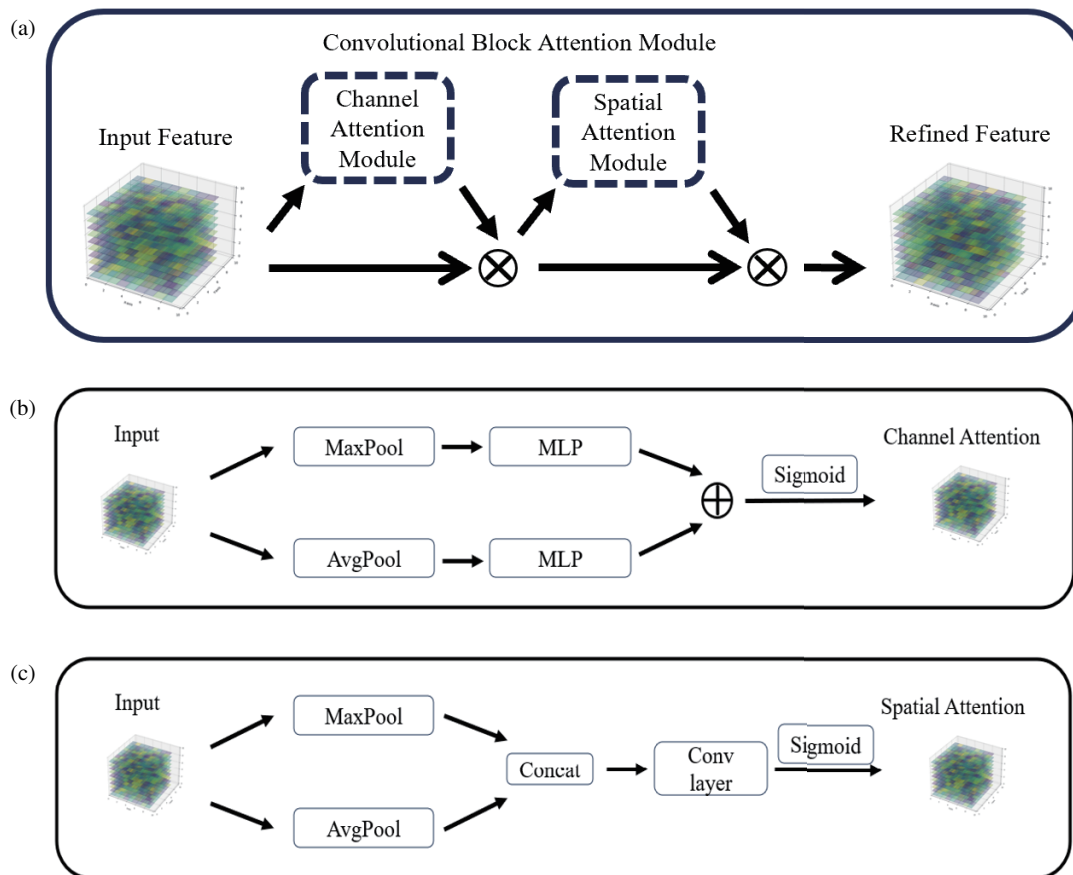
FIGURE 4. (a) The structure of the Convolutional Block Attention Module (CBAM). The input features pass through the channel attention module and the spatial attention module to adjust the weights of each channel and each spatial position in the input feature map. (b) The structure of the Channel Attention Module. (c) The structure of the Spatial Attention Module.

FIGURE 5. The recognition results of the algorithm. (a) displays the RGB images of the lymph node samples, where (1), (2), (4), (6), and (8) are normal lymph nodes, and the others are lymph nodes with metastatic tumors. (b) and (c) show the recognition results based on hyperspectral cube data, with an accuracy of 97.68%. (Black represents the background, green represents normal samples, and red represents metastatic tumor samples.).
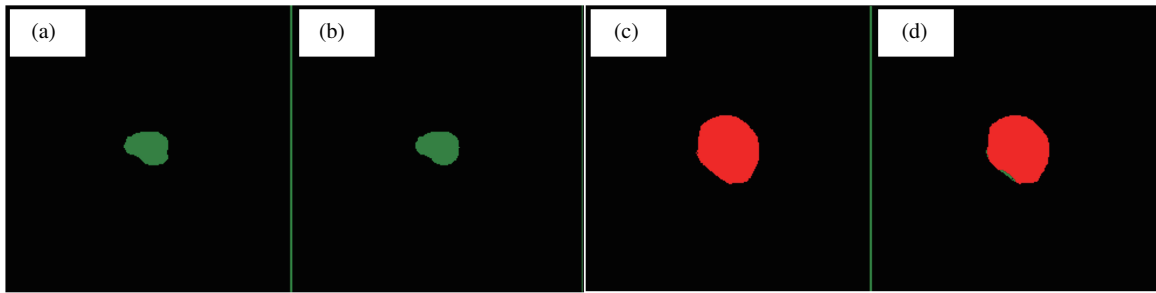
FIGURE 6. The application of the existing model to the classification of samples obtained using the multimodal hyperspectral laparoscope in the operating room. (a) and (c) represent the ground truth for negative and positive samples, respectively. (b) and (d) show the corresponding prediction results.

specimens. Following the preprocessing steps outlined in Section 2.1, we prepared the samples and utilized the hyperspectral laparoscopy to acquire hyperspectral data. Note that 6 new lymph nodes (including 1 with metastatic tumor and 5 normal lymph nodes) taken with the hyperspectral laparoscopy were added to the previous training set, and three new lymph nodes were used as the test set. The confusion matrix was calculated with pixel-by-pixel (instead of lymph node-by-node).

Using the previously established *ex vivo* sample model for prediction, we achieved a testing accuracy of 94%, with some of the prediction results illustrated in Figure 6. This demonstrates that our hyperspectral laparoscope system holds significant potential for the clinical diagnosis of metastatic lymph nodes.

Although this experiment involved only 80 samples, which may be considered as a small sample size, it still demonstrated the potential of the system in clinical label-free intraoperative real-time diagnosis of colorectal cancer lymph nodes.

4. SUMMARY AND OUTLOOK

In this work, we developed and applied a multi-modal hyperspectral imaging system and an improved U-Net algorithm to process multi-modal data. The algorithm incorporates a spatial attention module to enhance feature extraction and recognition accuracy. We tested the algorithm using a dataset of 27 lymph nodes, including 7 with metastatic tumors and 20 normal lymph nodes for training; and 19 lymph nodes, including 8 with metastatic tumors and 11 normal lymph nodes for testing. The results showed that the hyperspectral cube data achieved a significantly higher accuracy of 97.68%. To validate the practical clinical potential of our system, we integrated it with a commercial hyperspectral laparoscope to perform multimodal hyperspectral endoscopic detection. Using the model trained on *ex vivo* samples, we achieved a classification accuracy of 94%. These results demonstrate that our system outperforms conventional laparoscopic examinations and has significant potential for *in vivo* label-free diagnosis of lymph node metastasis in CRC.

While the current algorithm has shown promising results, further optimization can be explored to improve its performance. This may include refining the spatial attention module, incorporating temporal attention, or using more advanced deep learning architectures. The next step is to integrate the system into clinical workflows to validate its effectiveness in real-world scenarios. This will involve testing the algorithm on a larger and more diverse dataset of patient samples and collaborating with medical professionals to ensure its practical utility. We plan to investigate more sophisticated multimodal fusion techniques that can combine the strengths of both hyperspectral imaging and Raman imaging [14]. This could lead to even higher accuracy and more robust recognition of lymph node conditions. We may also utilize some existing advanced deep learning networks developed for RGB data and apply a 3-band iteration method to transfer knowledge learned from RGB data pretrained models to the hyperspectral domain [15].

DECLARATION OF COMPETING INTEREST

The authors declare that they have no known competing financial interests or personal relationships that could have appeared to influence the work reported in this paper.

REFERENCES

[1] Mohammadian-Hafshejani, A., "Global, regional, and national cancer incidence, mortality, years of life lost, years lived with disability, and disability-adjusted life-years for 29 cancer groups, 1990 to 2017: A systematic analysis for the global burden of disease study," *JAMA Oncology*, Vol. 5, No. 12, 1749–1768, 2019.

[2] Mannath, J. and K. Ragunath, "Role of endoscopy in early oesophageal cancer," *Nature Reviews Gastroenterology & Hepatology*, Vol. 13, No. 12, 720–730, 2016.

[3] Shaukat, A. and T. R. Levin, "Current and future colorectal cancer screening strategies," *Nature Reviews Gastroenterology & Hepatology*, Vol. 19, No. 8, 521–531, 2022.

[4] Yamazaki, Y., S. Kanaji, G. Takiguchi, N. Urakawa, H. Hasegawa, M. Yamamoto, Y. Matsuda, K. Yamashita, T. Matsuda, T. Oshikiri, *et al.*, "Preoperative endoscopic tattooing using india ink to determine the resection margins during totally laparoscopic distal gastrectomy for gastric cancer," *Surgery Today*, Vol. 51, 111–117, 2021.

[5] Jalaly, N. Y., N. Valizadeh, S. Azizi, F. Kamani, and M. Hassanzadeh, "Sentinel lymph node mapping and biopsy using radioactive tracer in gastric cancer," *ANZ Journal of Surgery*, Vol. 84, No. 6, 454–458, 2014.

[6] Kumar, S., R. Dhillon, S. Shah, D. C. White, and W. M. Rozen, "Patent Blue dye allergy and the deep inferior epigastric perforator free flap: A unique interaction," *Clinical Case Reports*, Vol. 6, No. 4, 581–584, 2018.

[7] Bove, S., S. M. Fragomeni, A. Romito, P. Rinaldi, D. Pagliara, D. Verri, I. Romito, I. Paris, L. Tagliaferri, F. Marazzi, *et al.*, "Techniques for sentinel node biopsy in breast cancer," *Minerva Surgery*, Vol. 76, No. 6, 550–563, 2021.

[8] Chao, C.-H., Z. Zhu, D. Guo, K. Yan, T.-Y. Ho, J. Cai, A. P. Harrison, X. Ye, J. Xiao, A. Yuille, *et al.*, "Lymph node gross tumor volume detection in oncology imaging via relationship learning using graph neural network," in *International Conference on Medical Image Computing and Computer-Assisted Intervention*, 772–782, 2020.

[9] Waterhouse, D. J., W. Januszewicz, S. Ali, R. C. Fitzgerald, M. d. Pietro, and S. E. Bohndiek, "Spectral endoscopy enhances contrast for neoplasia in surveillance of Barrett's esophagus," *Cancer Research*, Vol. 81, No. 12, 3415–3425, 2021.

[10] Guo, T., Z. Lin, X. Xu, Z. Zhang, X. Chen, N. He, G. Wang, Y. Jin, J. Evans, and S. He, "Broad-tuning, dichroic metagrating Fabry-Perot filter based on liquid crystal for spectral imaging," *Progress In Electromagnetics Research*, Vol. 177, 43–51, 2023.

[11] Yao, X., F. Cai, P. Zhu, H. Fang, J. Li, and S. He, "Non-invasive and rapid pH monitoring for meat quality assessment using a low-cost portable hyperspectral scanner," *Meat Science*, Vol. 152, 73–80, 2019.

[12] Yoon, J., J. Joseph, D. J. Waterhouse, A. S. Luthman, G. S. D. Gordon, M. D. Pietro, W. Januszewicz, R. C. Fitzgerald, and S. E. Bohndiek, "A clinically translatable hyperspectral endoscopy (HySE) system for imaging the gastrointestinal tract," *Nature Communications*, Vol. 10, No. 1, 1902, 2019.

[13] Kumashiro, R., K. Konishi, T. Chiba, T. Akahoshi, S. Nakamura, M. Murata, M. Tomikawa, T. Matsumoto, Y. Maehara, and M. Hashizume, "Integrated endoscopic system based on optical imaging and hyperspectral data analysis for colorectal cancer detection," *Anticancer Research*, Vol. 36, No. 8, 3925–3932, 2016.

[14] Jiao, C., J. Liao, and S. He, "An aberration-free line scan confocal raman imager and type classification and distribution detection of microplastics," *Journal of Hazardous Materials*, Vol. 470, 134191, 2024.

[15] Wang, L. and S. He, "A 3-band iteration method to transfer knowledge learned in RGB pretrained models to hyperspectral domain," *Progress In Electromagnetics Research M*, Vol. 128, 1–9, 2024.